Islamic Azad University

Journal of

Optoelectronical Nanostructures

Winter 2021 / Vol. 6, No. 1

Research Paper

The impact of the plasmon-exciton interaction on the optical characteristics of the hybrid system $NPVO_2 - QD - NPVO_2$

Abdolrasoul Gharaati*[,1], Ghasem Forozani[1], Esmail Salari Sardoi[1]

[1]Department of Physics, Payame Noor University, Tehran, Iran

Received:
Revised:
Accepted:
Published:

Use your device to scan and read the article online

DOI:

Keywords:
Optical properties, Quantum dot, Hybrid system, Forster broadening, Exciton energy transfer.

Abstract:

In this paper, the optical characteristics of a plexitonic system comprising two $NPVO_2$ and one quantum dot (QD) were investigated. Both $NPVO_2$ and QD have unique optical properties on their own and their combination in the hybrid system $NPVO_2$-QD-$NPVO_2$ can lead to interesting phenomena. In this method, when the $NPVO_2$ and QD nanoparticles and their resonance frequencies are close to each other, due to the interaction between $NPVO_2$ plasmons and QD excitons, the optical characteristics of QD change. In this paper, the changes in the optical properties of QD near $NPVO_2$, a crystalline material that transitions from a semiconducting phase to a metallic phase at a critical temperature, were studied. The results showed that the proximity of $NPVO_2$ to a QD caused an energy shift and an absorption peak which are also used in sensor applications. Moreover, the Förster broadening as well as exciton energy transfer were also investigated. It was revealed that they changed due to the dipole-dipole interaction between plasmon and excitons.

Citation: First Author's Full Name, Second Author's Full Name, Third Author's Full Name. The effect of Cinnamon supplementation on lipid profile in response to aerobic exercise. **Journal of Optoelectronical Nanostructures.** 2020; 1 (1): 48-58

***Corresponding author:**
Address:
Tell: Email:

1. INTRODUCTION

Fundamental research in the field of nanophotonics primarily focuses on understanding the optical excitations induced by nanoscale materials and how the characteristics of these excitations depend on the size, shape, and arrangement of nanostructures. Two types of excitations that have garnered significant attention from researchers are plasmons in metallic nanostructures and excitons in molecular materials or semiconductors. Plasmons are the collective oscillations of free electrons in metals. The coupling of light with plasmon resonance has attracted considerable interest because it can concentrate light fields in volumes much smaller than the diffraction limit [1]. Excitons are bound pairs of electrons and holes in semiconductors or molecules, and they have gained considerable attention in semiconductor nanocrystals or quantum dots (QDs) due to their size-dependent frequency transitions and effective light emission [2].

Recent advancements in nanostructure fabrication techniques enable researchers to combine various nanoparticles with contrasting optical characteristics into multi-structured nanocomposites, offering exciting possibilities to modify or design specific optical processes in the constituent nanoparticles [1-3].

A substantial number of studies in this field have explored the interaction of excitonic systems in semiconductor QDs and plasmonic nanostructures, providing a wide range of opportunities to control the interaction of light and matter as well as the flow of electromagnetic energy [4-6].

Given that optical excitation occurs in the form of excitons and plasmons in quantum dots (QDs) and metal nanoparticles, respectively, QDs and metal nanoparticles are examined through quantum mechanics and classical mechanics, respectively. When an electric field is applied, the plasmons in the metal nanoparticle are excited, creating a field around the nanoparticle that enhances the local field nearby. This local field also excites the excitons in the QD, resulting in a coupling between the plasmon and exciton, which leads to various intriguing effects such as energy transfer, changes in exciton energy, interference, and an increase in the local field [7]. Theoretical studies on the metal nanoparticle-semiconductor QD (MNP-SQD) system have predicted Förster energy transfer facilitated by plasmons [8], modifications to spontaneous emission in semiconductor QDs [9], third-and fifth-order optical processes of tunable exciton-plasmon hybrid nanosystem [10], increase in the induced fluorescence of QD [11], tunnelling induced transparency [12], plasmonic two-photon switching phenomena [13], and control over energy transfer pathways in hybrid systems [14]. Numerous experimental studies have also been conducted on these combined systems. For instance, Mertens et al. demonstrated

polarization-selective enhancement of QD photoluminescence in silicon QDs coupled with silver nanoparticles [15]. Pons et al. developed a system comprising a CdSe-ZnS QD and a gold nanoparticle [16]. Vasa et al. constructed a hybrid metal-semiconductor nanostructure consisting of a GaAs quantum well on a gold substrate [17]. They reported a significant shift and broadening of the exciton resonance in the quantum well due to strong exciton-plasmon coupling. Additionally, they observed an increase in broadband electromagnetic absorption in a silicon film with a photonic crystal surface and a random gold groove reflector [18].

In this system, the Hamiltonian of the entire system, featuring two metal nanoparticles on either side of the QD, is first calculated. The electric field experienced by the QD consists of three components: one is the applied external field, while the other two are internal fields induced by the polarizations on both sides of the QD. Subsequently, using density matrix theory, the elements of the density matrix and the polarization of the QD are computed. Following this, the optical characteristics of the QD are examined.

In this paper, the optical properties of the $NPVO_2$-QD-$NPVO_2$ plexitonic system are investigated. First, $NPVO_2$ is introduced. Next , by controlling the temperature while maintaining the same structure, the changes in QD properties due to $NPVO_2$ can be observed.

2. THEORETICAL MODEL

VO_2 has garnered significant attention due to its reversibility and phase transition temperature (approximately 68 ℃) [19]. This structural phase involves a transition from the monoclinic phase (at low temperatures, where it acts as an insulator or weak semiconductor) to the tetragonal rutile phase (at high temperatures, where it behaves as a metallic material). Following the phase transition, the electrical conductivity changes by a factor of 3 to 5, and the optical properties undergo substantial alterations. Various optical, thermal, and electrical devices have been proposed based on the metal-to-insulator phase transition of VO_2 [20, 21].

The phase transition in VO_2 can be induced by various applied forces, including intense radiation, external electric fields, hydrostatic pressure, and tension [22, 23].

Until a few years ago, many studies focused on VO_2 thin film materials with a critical temperature of 68 ℃. Today, advancements in nanomaterial

production have led to the synthesis of VO_2-based nanoparticles using various chemical and physical methods. Moreover, their critical temperature has been reduced to room temperature. The two contrasting phases of VO_2 and their mixture can be modeled using a temperature-dependent filling fraction, which is 0 for the semiconducting phase and 1 for the metallic phase [24]. At intermediate temperatures (during phase transitions), matter exists as a mixture of two phases, modeled using effective medium theory, specifically the Maxwell-Garnett theory, to derive the effective dielectric function ε_{VO_2} [23]:

$$\varepsilon_{VO_2} = \varepsilon_{semi} \frac{(\varepsilon_{met}(1+2f) - \varepsilon_{semi}(2f-2))}{(\varepsilon_{met}(1-f) + \varepsilon_{semi}(2+f))} \quad (1)$$

in which f f is the filling factor controlling the phase transition in $NPVO_2$. Fig. 1 shows the temperature changes of f as a Bessel function for cooling and heating modes in the vicinity of the critical temperature.

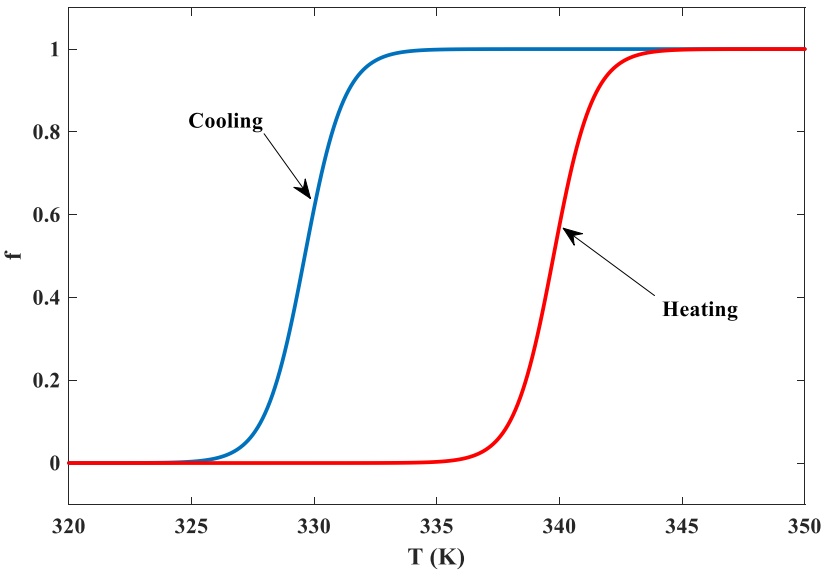

Fig. 1. The filling factor of VO_2 as a function of temperature [22].

ε_{semi} is the dielectric function of VO_2 in the semiconducting phase ($f=0$), whereas ε_{met} is the dielectric functions of VO_2 in metallic phase ($f=1$) as shown below [23].

$$\varepsilon_{semi}(\omega)=1+\frac{(\varepsilon_n(i\infty)-1)}{(1-\omega^2/(\omega_\infty^2))}+\sum_{(i=1)}^{7}\frac{S_{n.i}}{1-\frac{\omega^2}{\omega_{n,i}^2}-i\frac{\Gamma_{n.i}\omega}{\omega_{n,i}^2}} \quad (2)$$

$$\varepsilon_{met}(\omega)=1-\frac{\omega_{p,\tilde{n}}^2}{\omega(\omega+i\gamma_{\tilde{n}})}+\frac{\varepsilon_{\tilde{n}}(i\infty)-1}{1-\frac{\omega^2}{\omega_\infty^2}}+\sum_{i=1}^{4}\frac{S_{\tilde{n}.i}}{1-\frac{\omega^2}{\omega_{n,i}^2}-i\frac{\Gamma_{\tilde{n}.i}\omega}{\omega_{n,i}^2}} \quad (3)$$

where $\varepsilon_n(i\infty)=3.95$, $\omega_{p,\tilde{n}}=3.33eV$, $\gamma_{\tilde{n}}=0.66eV$, $\varepsilon_{\tilde{n}}(i\infty)=4.26$, and $\omega_\infty=15eV$. The other parameters in Eqn. (2) and Eqn. (3) are given in [21].

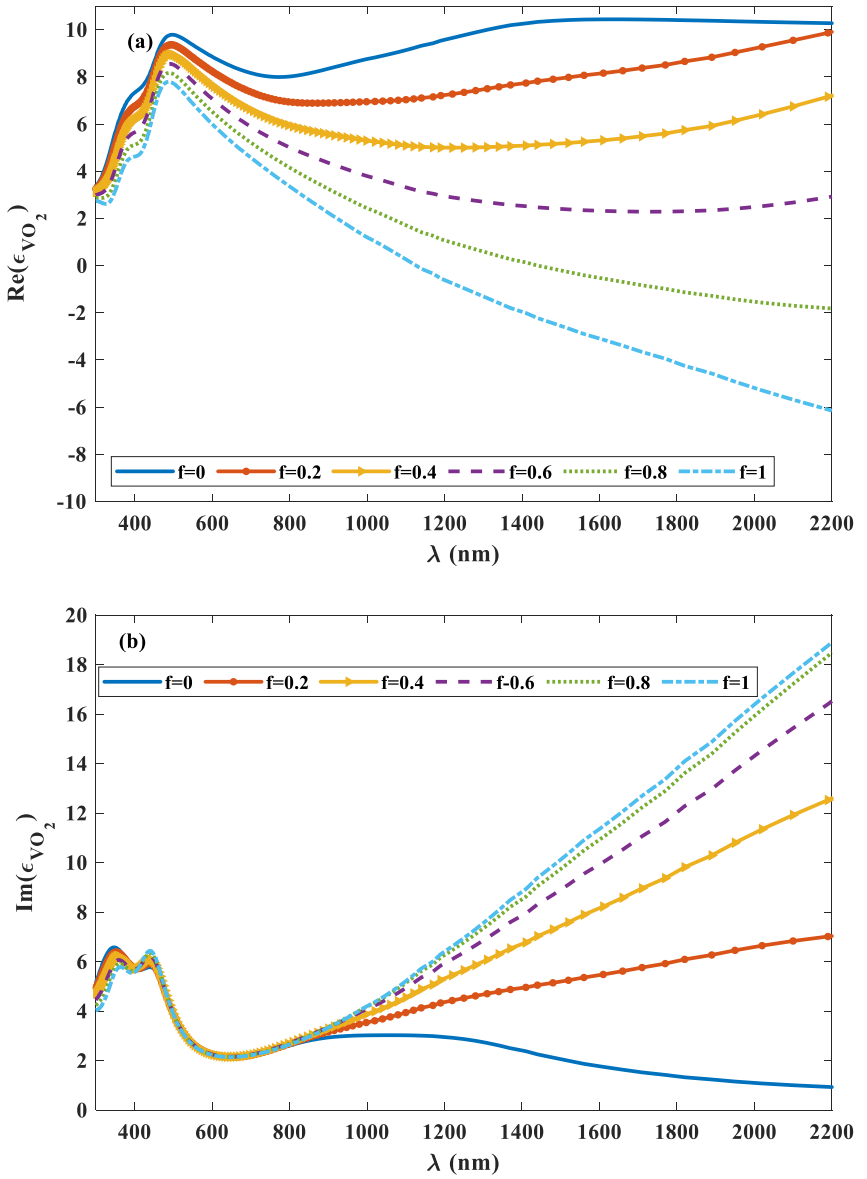

Fig. 2. a) The real and b) imaginary parts of the effective dielectric function ε_{VO_2} versus the incident wavelength for different filling fraction values.

Fig. 2 illustrates the real and imaginary parts of the dielectric function versus the incident wavelength to show the dependence of the effective dielectric function ε_{VO_2} on the filling fraction. Figure 2 (a) indicates that the real part of the dielectric function is negative for wavelengths above 1080 nm (energy = 1.14 eV). Consequently, at lower energies and higher filling fractions, VO_2 behaves similarly to a metal with a negative real part, leading to significant changes in the polarizability of $NPVO_2$ in the infrared region. These findings align well with previous studies on the optical characteristics of VO_2 .

$NPVO_2$ is described by the multipole moment induced by an energy-dependent scalar polarizer. This polarizability could be managed by the ambient temperature which changes the filling fraction. The multipole polarizability could be given as [21]:

$$\beta_n = \frac{\varepsilon_{VO_2} - \varepsilon_b}{\varepsilon_{VO_2} + \frac{n+1}{n}\varepsilon_b} \tag{4}$$

where n stands for the multipole order so that the lowest order (n=1) represents the dipole order. ε_b is the dielectric function of the local background.

To demonstrate the dependence of the polarization of $NPVO_2$ on the filling fraction, using finite element method for one $NPVO_2$ with a size of 40 nm, Fig. 3 (a) shows inside the silica material for different filling fraction values including metallic and semiconducting phases. Electromagnetic simulations were conducted using the finite-element method in COMSOL Multiphysics. The electromagnetic module solved for electric field distribution, employing perfectly matched layers (PMLs) at a distance of half the maximum electromagnetic wavelength from the unit cell to prevent back reflection from exterior boundaries. PMLs at the around of the unit cell absorb the excited mode from the source port and any higher order modes produced by the periodic structure. In the metallic phase, the maximum absorption cross-section occurs at 1140 nm (energy=1.08 eV), whereas the maximum absorption cross-section in the semiconducting phase is at lower wavelengths. At this energy level, the amounts of absorption cross-section for metal and semiconductor are $\sigma_{abs} = 621\,nm^2$ and, $\sigma_{abs} = 125\,nm^2$ respectively. According to the results, the semiconductor-to-metal transition increases about 5 times in the infrared region of the cross-section.

Figs. 3 (b) and 3 (c) illustrate the increase in the near-field at 1140 nm, shown as the amplitude of the scattered field relative to the incident field. The peak intensities for the metallic and semiconducting phases are 2.2 and 1.5, indicating

a symmetrical distribution. Notably, maximum absorption, based on the quasi-static approximation, occurs at 1140 nm, aligning with the resonance wavelength of surface plasmons in the metallic phase of $NPVO_2$.

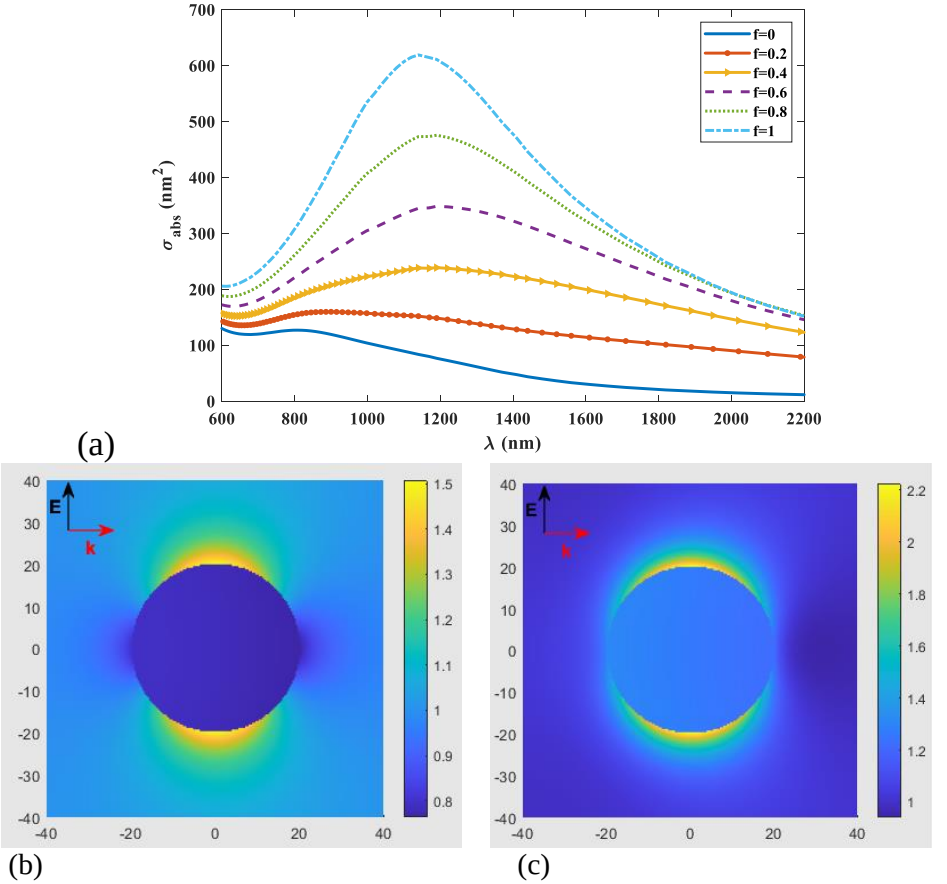

Fig. 3. (a) Calculations of the finite elements of the absorption cross-section versus the wavelength for $NPVO_2$ in a silica medium. (b) and (c) Field enhancement at the wavelength of 1140 nm for the semiconducting and metallic phases, respectively.

A. The $NPVO_2$ - QD - $NPVO_2$ hybrid system

In this section, the $NPVO_2$-QD-$NPVO_2$ hybrid system is discussed. QD optical excitations are classified as excitons, while nanoparticle excitations ($NPVO_2$) correspond to surface polaritons and surface plasmon polaritons in

semiconducting and metallic phases, respectively. When these nanoparticles with distinct properties are placed adjacent to each other and subjected to an external field, the plasmons and excitons are excited, leading to Coulomb interactions between them. This dipole-dipole interaction becomes notably strong when the nanoparticles' resonance frequencies are closely aligned. The inclusion of metal nanoparticles aims to enhance the interaction strength, while the plasmonic field generated nearby serves to improve both linear and non-linear optical properties of the semiconductor QD.

Fig. 4 shows the QD with radius a between two $NPVO_2$ with radii R_1 and R_2. The center-to-center distance of the QD from the two nanoparticles is indicated by d_1 and d_2, respectively. The system is placed in a background field with dielectric constant ε_b.

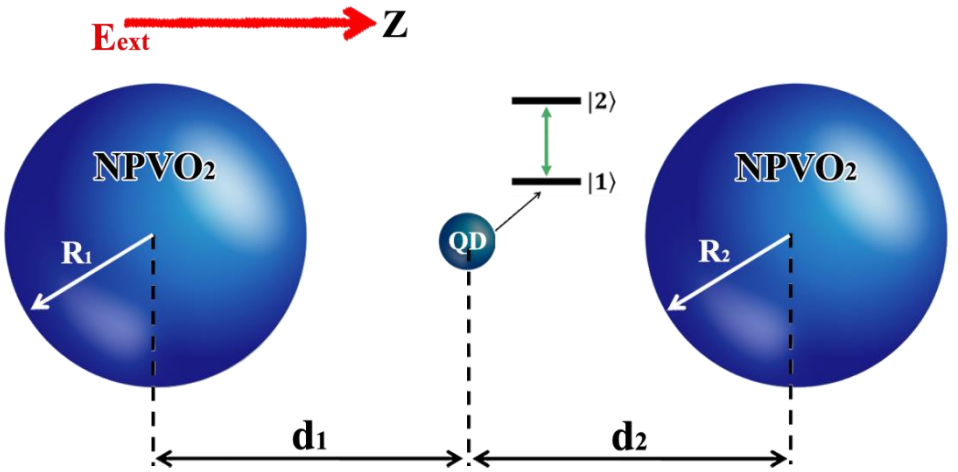

Fig. 4. The schematic of a $NPVO_2$-QD-$NPVO_2$ hybrid system with the $NPVO_2$ resonance frequency in the metallic phase which is close to the exciton transition frequency $|1\rangle \leftrightarrow |2\rangle$.

B. The motion equations of the $NPVO_2$ - QD - $NPVO_2$ system

According to Fig. 4, when the external electromagnetic field $E_{ext}(t) = E_0(e^{i\omega t} + e^{-i\omega t})$ is applied to the system, the plasmons and excitons are excited in $NPVO_2$ and QD, respectively. In addition, the QD senses two other

induced fields caused by the polarization of $NPVO_2$. Therefore, the QD field is given below [25]:

$$E_{QD} = \frac{1}{\varepsilon_{eff_{QD}}}\left(E_{ext} + E^{ddi}_{NPVO_2,1} + E^{ddi}_{NPVO_2,1}\right) \tag{5}$$

where $\varepsilon_{eff_{QD}} = \frac{2\varepsilon_b + \varepsilon_s}{3\varepsilon_b}$, while $E^{ddi}_{NPVO_2,j} = \frac{1}{4\pi\varepsilon_b}\frac{S_a P_{NPVO_2,j}}{R_j^3}(j = 1,2)$ indicates the induced field produced by $NPVO_2$ which has an interaction with the QD. The polarization of each $NPVO_2$ is given by $P_{NPVO_2,j} = 4\pi\varepsilon_b a_j^3[\gamma_j(\omega)\bar{E}_{NPVO_2,j}e^{-i\omega t} + \gamma_j^*(\omega)\bar{E}_{NPVO_2,j}e^{i\omega t}]$ where γ_j is the dipole polarizability of $NPVO_2$ for each nanoparticle j. $E_{NPVO_2,j}$ is the total field of each $NPVO_2$ which in addition to the external field has two terms from the field caused by the QD polarization and the field caused by another $NPVO_2$ which are written as follows [25]:

$$\begin{aligned} E_{NPVO_2,1} &= E_{ext} + \frac{S_a P_{QD}}{4\pi\varepsilon_b\varepsilon_{eff_{QD}}R_1^3} + \frac{S_a P_{NPVO_2,2}}{4\pi\varepsilon_b\varepsilon_{eff_{NPVO_2,2}}(R_1^3+R_2^3)^3}, \\ E_{NPVO_2,2} &= E_{ext} + \frac{S_a P_{QD}}{4\pi\varepsilon_b\varepsilon_{eff_{QD}}R_2^3} + \frac{S_a P_{NPVO_2,1}}{4\pi\varepsilon_b\varepsilon_{eff_{NPVO_2,1}}(R_1^3+R_2^3)^3} \end{aligned} \tag{6}$$

Using the density matrix, QD polarization could be presented based on its off-diagonal elements as $P_{QD} = \mu(\rho_{12} + \rho_{21})$ where μ is the transition dipole moment, $\rho_{12} = \rho_{12}e^{-i\omega t}$ and $\rho_{21} = \rho_{21}e^{i\omega t}$ are the density matrix elements that change with time, and $\varepsilon_{eff_{NPVO_2,j}} = \frac{2\varepsilon_b + \varepsilon_{NPVO_2,j}(\omega)}{3\varepsilon_b}(j = 1,2)$.

By performing mathematical calculations, the total field of the QD is obtained as follows [10,11]:

$$E_{QD} = \frac{\hbar}{\mu}\left[(\Omega + \eta\rho_{12})e^{-i\omega t} + (\Omega + \eta\rho_{21})e^{i\omega t}\right] \tag{7}$$

where Ω and η are respectively the normalized Rabi frequency and the self-interaction of the QD which are given as follows:

$$\Omega = \frac{E_0 \mu}{2\hbar \varepsilon_{eff_{QD}}} \left\{ 1 + \frac{\frac{S_a a_1^3 \gamma_1}{R_1^3} \left(1 + \frac{S_a a_2^3 \gamma_2}{\varepsilon_{eff_{NPVO_2},2} (R_1 + R_2)^3} \right)}{1 - \frac{S_a^2 a_1^3 \gamma_1 a_2^3 \gamma_2}{\varepsilon_{eff_{NPVO_2},1} \varepsilon_{eff_{NPVO_2},2} (R_1 + R_2)^3}} + \frac{\frac{S_a a_2^3 \gamma_2}{R_2^3} \left(1 + \frac{S_a a_1^3 \gamma_1}{\varepsilon_{eff_{NPVO_2},1} (R_1 + R_2)^3} \right)}{1 - \frac{S_a^2 a_1^3 \gamma_1 a_2^3 \gamma_2}{\varepsilon_{eff_{NPVO_2},1} \varepsilon_{eff_{NPVO_2},1} (R_1 + R_2)^3}} \right\},$$

$$\eta = \frac{S_a^2 \mu^2}{4\pi \varepsilon_b \hbar \varepsilon_{eff_{QD}}^2} \left\{ \frac{\frac{a_1^3 \gamma_1}{R_1^3} \left(\frac{1}{R_1^3} + \frac{S_a a_2^3 \gamma_2}{\varepsilon_{eff_{NPVO_2},2} R_2^3 (R_1 + R_2)^3} \right)}{1 - \frac{S_a^2 a_1^3 \gamma_1 a_2^3 \gamma_2}{\varepsilon_{eff_{NPVO_2},1} \varepsilon_{eff_{NPVO_2},2} (R_1 + R_2)^3}} + \frac{\frac{a_2^3 \gamma_2}{R_2^3} \left(\frac{1}{R_2^3} + \frac{S_a a_1^3 \gamma_1}{\varepsilon_{eff_{NPVO_2},2} R_1^3 (R_1 + R_2)^3} \right)}{1 - \frac{S_a^2 a_1^3 \gamma_1 a_2^3 \gamma_2}{\varepsilon_{eff_{NPVO_2},1} \varepsilon_{eff_{NPVO_2},2} (R_1 + R_2)^3}} \right\}$$

(8)

The Hamiltonian of the QD with ground $|1\rangle$ and excited $|2\rangle$ states, whose energy difference is $\hbar\omega_0$, is expressed as follows [25]:

$$H_{QD} = \hbar\omega_0 \hat{a}^\dagger \hat{a} - \mu . E_{QD} (\hat{a} + \hat{a}^\dagger) \tag{9}$$

where $\hat{a}^\dagger$ is the creation operator of the ground state and $\hat{a}$ is the annihilation operator of the excited state.

Using the density matrix method and the equation of motion for the density matrix operator ($\frac{\partial \rho_{nm}(t)}{\partial t} = -\frac{i}{\hbar}\left[H_{QD}, \rho(t)\right]_{nm} + \Gamma(\rho),$) we present the density matrix elements to facilitate the investigation of energy transfer and QD behavior [26]:

$$\frac{d\Delta_\rho}{dt} = -2\Gamma_{21}\rho_{22} + 2i((\Omega + \eta\rho_{21})\rho_{12} - (\Omega + \eta\rho_{21})^* \rho_{21}) \tag{10}$$

$$\frac{d\rho_{21}}{dt} = -[i(\Delta_k - \eta_R \Delta_\rho) + (\gamma_{21} + \eta_I \Delta_\rho)]\rho_{21} + i\Omega\Delta_\rho \tag{11}$$

where $\Delta_\rho = \rho_{22} - \rho_{11}$ indicates the difference between the first two states in the QD and $\Delta_k = \omega_0 - \omega$ is the difference between the exciton transition and the energy of the laser field. $\eta_I \Delta_\rho$ and $\eta_R \Delta_\rho$ respectively show the Förster

broadening factor of the exciton transition and the energy shift of this transition where $\eta_R = Real(\eta)$ and $\eta_I = Imag(\eta)$.

Moreover, in this structure, the absorption of the QD due to the transition $|2\rangle \leftrightarrow |1\rangle$ is calculated through the imaginary part of. $Im(\rho_{21})$ To solve the dynamic equations (10) and (11), the fourth-order Rang-Kutta method is used.

3. DISCUSSION AND NUMERICAL RESULTS

In this part, the effect of $NPVO_2$ in different phases on the optical properties of QD in the $NPVO_2$-QD-$NPVO_2$ plexitonic system is studied. The following parameters are employed in our calculations: $a = 4nm$ and $R_1 = R_2 = 20\ nm$. $\Gamma_{12} = 1.25\ ns^{-1}$ is the spontaneous radiative decay [21]. The dielectric constant of the background is $\varepsilon_b = 2.25$. Using Mie theory, the absorption cross-section for the metallic phase of $NPVO_2$ at $\omega_{21} = 1.08\,eV$ ($\lambda = 1140\,nm$) has a resonant peak which indicates the excitation of surface plasmon polaritons. Given that the peak of absorption in the metallic phase of $NPVO_2$ is in the infrared region, the QD Ag_2S, where the excitonic transition $|1\rangle \rightarrow |2\rangle$ is located ($\omega_{21} = 1.08\,eV$), is considered. Silver sulfide (Ag_2S) QD is considered as a suitable and remarkable candidate for our study. This choice is due to the fact that silver sulfide has been experimentally proven to have very interesting absorption properties in the infrared (IR) region [23]. In particular, in this region we note the excited transition $|2\rangle \leftrightarrow |1\rangle$, which corresponds to the characteristic resonance energy. This resonance energy is specifically detectable with the $NPVO_2$ surface plasmon resonance in the metallic phase.

Fig. 5 shows the imaginary part ρ_{21} which represents the absorption spectra of the QD for different phases (different fs where $f = 0$ stand for the semiconducting phase and $f = 1$ represents the metallic phase) versus Δ_k. In this figure, the radii of the QD and nanoparticles are constant, with the filling fraction f changing only with temperature. The figure illustrates two $NPVO_2$, which alter both the energy shift and the absorption profile near the energy transition. As f increases, the absorption profile decreases and shifts further, and the bandwidth of the absorption spectrum also expands. This behavior can be attributed to the interactions between the QD and the nanoparticles, which are strongly influenced by the local environment and the thermal dynamics of the system. As the temperature rises, the increased filling fraction f leads to enhanced electron-phonon coupling, which in turn modifies the optical properties of the hybrid system.

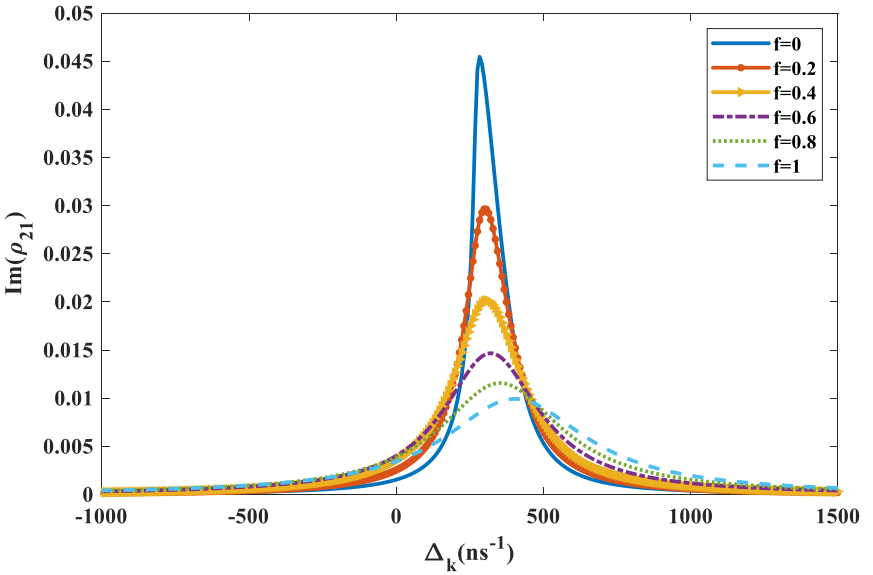

Fig. 5. The imaginary part of ρ_{21} indicating the absorption spectra of the QD versus Δ_k for different f .

To investigate the impact of the nanoparticles on the optical characteristics of the QD, Fig. 6 illustrates the imaginary part of ρ_{21} for three cases: (1) two $NPVO_2$ located on the two sides of the QD ($NPVO_2$-QD-$NPVO_2$); (2) a hybrid system with only one nanoparticle on one side of the QD ($NPVO_2$-QD); (3) a single QD. The results indicate that with the presence of two $NPVO_2$ in the semiconducting phase, there is a strong coupling as a result of the dipole/multipole interaction and that the absorption spectrum owing to the induced field which is in phase with the Rabi frequency shows a blue shift.
In (2) or (3) where a nanoparticle is located on one side of the quantum dot or the quantum dot is single and considering that $Im(\rho_{21})$ represents the absorption of the system. cases of (2, 3) is in very good agreement with previous work [21] that calculated the absorption of $NPVO_2$-QD hybrid system.

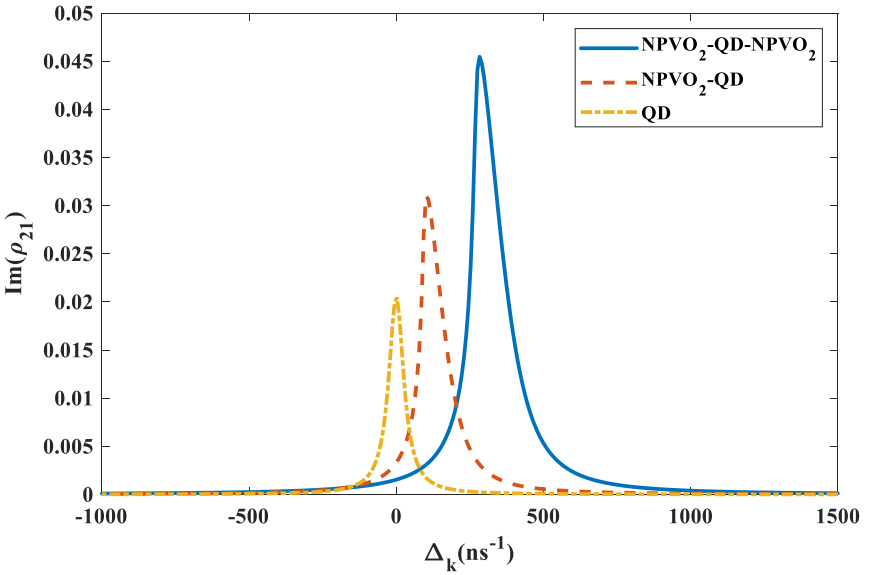

Fig. 6. The imaginary part of ρ_{21} versus the tunable exciton frequency and laser field energy for the three different states of the presence or absence of $NPVO_2$.

Figure 7 illustrates how temperature changes affect field enhancement in the strong-field region. The results indicate significant coupling in the semiconducting phase due to dipole/multipole interactions. The field is what the QD senses, and it is shown that there is no field enhancement when $\Delta_k = 0$. In the semiconducting phase, the field enhancement is about 5.5 times in the transition energy difference of $285\, ns^{-1}$. As f increases, the field enhancement peak diminishes and energy shifts further.

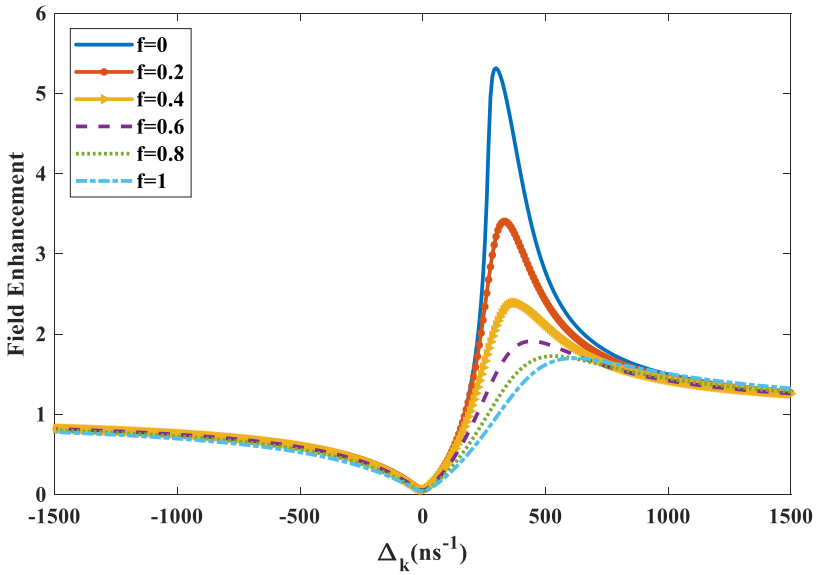

Fig. 7. The field enhancement of the $NPVO_2$-QD-$NPVO_2$ hybrid system based on the transition energy difference.

To investigate the behavior of $\eta_R \Delta_\rho$ when the $NPVO_2$-QD-$NPVO_2$ hybrid system is considered, it is plotted in Fig. 8 for different phases versus a frequency close to the transition frequency.

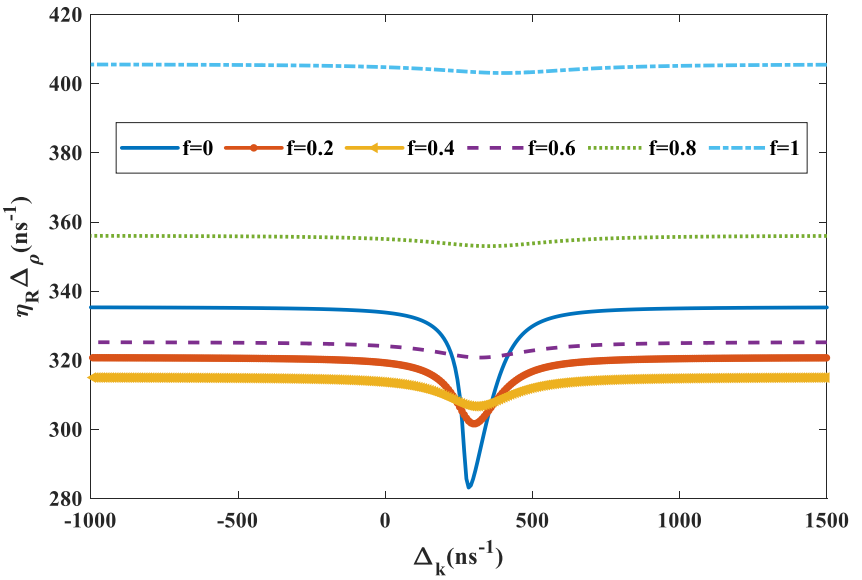

Fig. 8. The exciton transition energy shift ($\eta_R\Delta_\rho$) versus the Δ_k .

The figure shows that as f increases, the exciton transition energy shift also increases, resulting in a blue shift. At $f=0$, near the $|1\rangle \leftrightarrow |2\rangle$ transition ($\Delta_k = 285\, ns^{-1}$), the lowest exciton transition energy shift occurs. In contrast, when f=1 and frequencies are away from the $|1\rangle \leftrightarrow |2\rangle$ resonance, the exciton transition energy shift reaches approximately 405 ns^{-1}.

The effect of phase change as an effective parameter can be shown in the broadening of Förster energy. This process is normalized by the exciton population in the presence of quantum coherence. Therefore, Fig. 9 shows the parameter $\eta_I\Delta_\rho$ for the strong-field regime. The effect of this parameter is expressed in Eq. (12). As f increases, the Förster -enhanced broadening factor due to dipole/multipole also rises, changing from 41 ns^{-1} to 275 ns^{-1} as f shifts from 0 to 1, even at frequencies away from resonance.

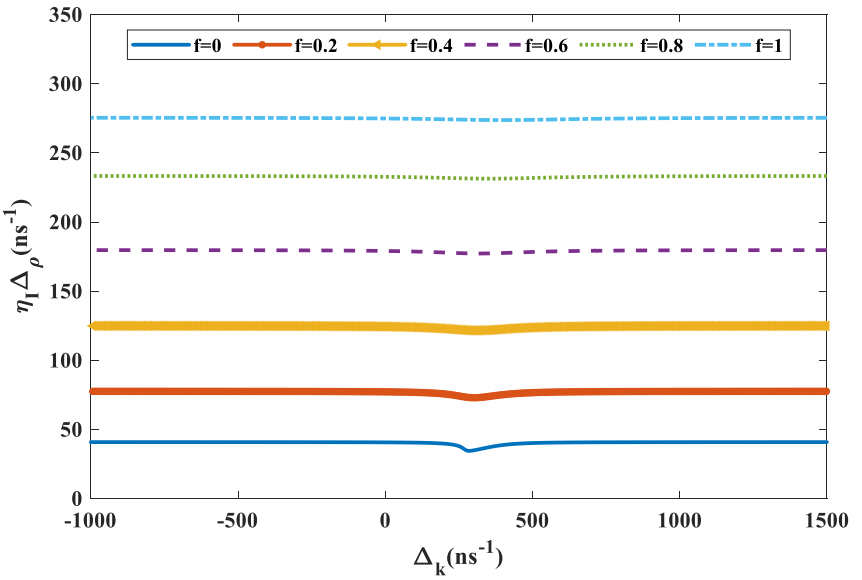

Fig. 9. Forster-enhanced broadening factor ($\eta_I \Delta_\rho$) according to the tunability of the exciton energy transition and the laser field ($\Delta_k = 0$).

4. CONCLUSION

One method for enhancing the optical characteristics of QDs is to incorporate nanoparticles into them. In this approach, the interaction between plasmons and excitons leads to changes in the optical properties of the QD. In this study, NPVO2 nanoparticles were employed. A notable finding was that with $NPVO_2$ present on both sides of the QD in the strong-field region, the absorption profile altered, resulting in an absorption peak and an energy shift in the resonance frequency of the QD. Furthermore, f significantly influenced the increase of the plasmonic field, exciton energy transition, and broadening. However, all these parameters were nearly zero at the transition frequency. For $NPVO_2$ nanoparticles, the field increased approximately five-fold at 285 ns^{-1}, indicating the excitation of plasmons in this region.

However, this study demonstrated how varying the temperature of $NPVO_2$ affects the optical characteristics of the plexitonic system while its physical parameters remain unchanged.

REFERENCE

[1] R. Vincent, H. Marinchio, J. J. Sáenz, and R. Carminati. *Local control of the excitation of surface plasmon polaritons by near-field magneto-optical Kerr effect*. Physical Review B. 90(24) (Dec. 2014) 241412. Available: https://doi.org/10.1103/PhysRevB.90.241412

[2] H. M. Ali, S. Abd-Elnabi, and K. Osman. *The intensity of the plasmon–exciton of three spherical metal nanoparticles on the semiconductor quantum dot having three external fields*. Plasmonics. 17(4) (Aug. 2022) 1633-1644. Available: https://doi.org/10.1007/s11468-022-01649-0

[3] M. C. Larciprete, D. Ceneda, D. Scirè, M. Mosca, D. Persano Adorno, and M. Centini. *Tunable IR perfect absorbers enabled by tungsten doped VO2 thin films*. APL Materials. 11(9) (Sep. 2023) 091107. Available: https://doi.org/10.1063/5.0164410

[4] L. Tan, X. Lu, L. Tang, K. Chen, J. Wang, and W. Huang. *Flexible composite film utilizing VO 2 self-adaptive photothermal and infrared radiative cooling for continuous energy harvesting*. Optics Express. 32(13) (Jun. 2024), 22675-22686. Available: https://doi: 10.1364/OE.523853

[5] A. Bile, D. Ceneda, V. E. Maryam, D. Scirè, and M. C. Larciprete. *Room-temperature tuning of mid-infrared optical phonons and plasmons in W-doped VO2 thin films*. Optical materials. 154 (Aug. 2024) 115732. Available: https://doi.org/10.1016/j.optmat.2024.115732

[6] M. A. Moghaddam, and N. Daneshfar. *Two-and three-photon absorption cross-section investigation in nanometer-sized heterodimer and heterotrimer structures*. The European Physical Journal Plus. 139(7) (Jul. 2024) 607. Available: https://doi.org/10.1140/epjp/s13360-024-05411-9

[7] E. Paspalakis, S. Evangelou, and A. F. Terzis. *Control of excitonic population inversion in a coupled semiconductor quantum dot–metal nanoparticle system*. Physical Review B. 87(23) (Jun. 2013) 235302. Available: https://doi.org/10.1103/PhysRevB.87.235302

[8] R. D. Artuso, and G. W. Bryant. *Optical response of strongly coupled quantum dot− metal nanoparticle systems: double peaked fano structure and bistability*. Nano letters. 8(7) (Iul. 2008) 2106-2111. Available: https://doi.org/10.1021/nl800921z

[9] Y. Fedutik, V.V. Temnov, O. Schöps, U. Woggon, and M.V Artemyev. *Exciton-plasmon-photon conversion in plasmonic nanostructures*. Physical review letters. 99(13) (Sep. 2007) 136802. Available: https://doi.org/10.1103/PhysRevLett.99.136802

[10] N. Daneshfar, and M. Mohammadbeigi. *Theoretical study of the nonlinear optical effects in tunable plasmon–exciton hybrid nanosystems: third-and fifth-order optical processes*. The European Physical Journal Plus. 138(5) (May 2023) 404. Available: https://doi.org/10.1140/epjp/s13360-023-04020-2

[11] J. Yi, X. Han, X. Chen, C. Liu, and Y. Luo. *The enhanced two-photonexcited fluorescence of CdSe quantum dots on the surface of au island films from surface Plasmon resonance*. Thin Solid Films. 521 (Oct. 2012) 112-114. Available: https://doi.org/10.1016/j.tsf.2012.02.041

[12] S. G. Kosionis, E. Paspalakis. *Tunneling induced transparency and slow light in an asymmetric double quantum dot molecule—Metal nanoparticle hybrid*. Journal of Applied Physics. 134(24) (Dec. 2023) 243107. Available: https://doi.org/10.1063/5.0174151

[13] . V. Bragas. *A nonlinear switching mechanism in quantum dot and metallic nanoparticle hybrid systems. Advanced Optical Materials*. 1(6) (Jun. 2013) 460-467. Available: https://doi.org/10.1002/adom.201300105

[14] A. Hatef, S. M. Sadeghi, S. Fortin-Deschênes, E. Boulais, and M. Meunier. *Coherently-enabled environmental control of optics and energy transfer pathways of hybrid quantum dot-metallic nanoparticle systems*. Optics express. 21(5) (Mar. 2013) 5643-5653. Available: https://doi.org/10.1364/OE.21.005643

[15] H. Mertens, J. S. Biteen, H. A. Atwater, and A. Polman. *Polarization-selective plasmon-enhanced silicon quantum-dot luminescence*. Nano letters. 6(11) (Nov. 2006) 2622-2625. Available: https://doi.org/10.1021/nl061494m

[16] T. Pons, I. L. Medintz, K. E. Sapsford, S. Higashiya, A. F. Grimes, D. S. English, and H. Mattoussi. *On the quenching of semiconductor quantum dot photoluminescence by proximal gold nanoparticles*. Nano letters. 7(10) (Oct. 2007) 3157-3164. Available: https://doi.org/10.1021/nl071729+

[17] P. Vasa, R. Pomraenke, S. Schwieger, Y. I. Mazur, V. Kunets, and G. Salamo. *Coherent exciton–surface-plasmon-polariton interaction in hybrid metal-semiconductor nanostructures*. Physical review letters. 101(11) (Sep. 2008)116801. Available: https://doi.org/10.1103/PhysRevLett.101.116801

[18] S. Rashidi, S. R. Entezar. And A. Rashidi. *Kerr-nonlinearity-assisted NIR nonreciprocal absorption in a VO_2-based core–shell composite integrated with 1D nonlinear multilayers*. Applied Optics. 60(28) (Oct. 2021) 8651-8658. Available: https://doi: 10.1364/AO.438938

[19] A. Rashidi. *Study of temperature distribution in a metallic nanograting based on a Kerr nonlinear material irradiated by a nanosecond pulsed*

laser. Iranian Journal of Physics Research. 23(4) (Feb. 2024) 621-628. Available: https://doi.org/10.47176/ijpr.23.4.11778

[20] S. A. Imam, K. M. Ishtiak and Q. D. Khosru. *Modelling a near perfect temperature tunable multiband VO2 based photonic-plasmonic absorber within visible and near infrared spectra*. Results in Engineering. 18 (Jun. 2023)101084. Available: https://doi.org/10.1016/j.rineng.2023.101084

[21] A. Hatef, N. Zamani, W. Johnston. *Coherent control of optical absorption and the energy transfer pathway of an infrared quantum dot hybridized with a VO_2 nanoparticle*. Journal of Physics: Condensed Matter. 29(15) (Mar. 2017) 155305. Available: https://doi.org/10.1088/1361-648X/aa61ee

[22] U. K. Chettiar, and N. Engheta. *Modeling vanadium dioxide phase transition due to continuous-wave optical signals*. Optics Express. 23(1) (Jan. 2015) 445-451. Available: https://doi.org/10.1364/OE.23.000445

[23] T. Kikuzuki, and M. Lippmaa. *Characterizing a strain-driven phase transition in VO_2*. Applied Physics Letters. 96(13) (Mar. 2010) 132107. Available: https://doi.org/10.1063/1.3380599

[24] H. T. Kim, Y. W. Lee, B. J. Kim, B. G. Chae, S. J. Yun, S. J., and Y. Lim. *Monoclinic and correlated metal phase in VO2 as evidence of the Mott transition: coherent phonon analysis*. Physical review letters. 97(26) (Dec. 2006) 266401. Available: https://doi.org/10.1103/PhysRevLett.97.266401

[25] N. Zamani, H. Nadgaran, and A. Hatef. *The effect of quantum correction for the dielectric function on the optical properties of a plasmon–exciton–plasmon hybrid system*. *The European Physical Journal D*. 75 (Jan 2021) 1-7. Available: https://doi.org/10.1140/epjd/s10053-021-00053-3

[26] M. C. Ko, N. C. Kim, C. J. Jang, G. J. Kim, Z. H. Hao and Q. Q Wang. *Control of the Optical Response of an Artificial Hybrid Nanosystem Due to the Plasmon-Exciton Plasmon Coupling Effect*. arXiv preprint arXiv:1708. (Aug. 2017) 06636 Available: https://doi.org/10.48550/arXiv.1708.06636